SUPPLEMENTARY MATERIAL

Figure S1. *P. patens* FLVA/B protein sequences similarity with FLV1/3.
Detail of the alignment of *P. patens* FLVA (XP_001759251.1) and FLVB (XP_001756079.1) proteins with FLV1 (sll1521), FLV2 (sll0219), FLV3 (sll0550) and FLV4 (sll0217) isoforms of *Synechocystis* PCC6803. The two residues characterizing *Synechocystis* FLV1-3 isoforms, believed to be involved in stabilization of NADPH binding (11), are marked with asterisks (*) and highlighted in yellow. These two residues are conserved in *P. patens* FLVA/B.

```
                610        620        630        640        650        660
          ....|....| *...|....| ....|....| ....|....| ....|...*| ....|....|
FLV1      SQATFSPPGL TVAVAKERAI ESLLHKNSCF VLNILQEGNH LGLMKHFLKP FAPGGDRFAD 535
FLV2      SQASFTPPGI MLAIPGEFDA YGLAGQNKAF VLNLLQEGRS VRRHFDHQPL PKDGDNPFSR 531
FLV3      SQASFNPPGF TVAVAKDRAI ESLMQVGDRF VLNILEEGNY QILMKHFLKR FPPGADRFAG 510
FLV4      IQGSFEPLGI VIAVAKDRAI ESLLHPGDTF VLNVLEEDNY QSLMRHFLLR FPPGADRFAG 515
PpFLVA    SQASFVPPGI TIAVAKDRAV EGLILTGSKF AISVLGQGKS GPVSKQLLKP FKPGENRLDG 660
PpFLVB    SQASFKPLGI TIAVAKDRAI ESLMQVGDTF VLNCLEEGKY APLMKHFLKR FPAGADRFEG 584
```

Figure S2. Construct design and verification of *FLVA* or *FLVB* gene disruption in selected *flva* KO and *flvb* KO lines.

A) Scheme of the construct used for the generation of *flva* KO plants. Genomic region of *FLVA* gene is schematized in the upper part (*FLVA WT locus*), with exons shown as black boxes. Grey shadows represent the genomic regions included in the targeting construct and therefore exploited for homologous recombination. Below is shown the construct for *FLVA* gene disruption: the gene providing resistance to hygromicin B (HygB) is located in between genome homologous regions (grey shadows). The *flva* KO locus after the homologous recombination event is also outlined. Arrows (not proportional to primer size) indicate the position of primers employed for *flva* KO generation and screening, listed in Table S2. The same approach was used for *flvb* KO strain generation.

B) Verification of *FLVA/B* gene disruption in genomic DNA of selected *flva* KO and *flvb* KO resistant lines. Amplification of the left (LB) and right (RB) borders is possible only in the case of resistance cassette integration in *flva* or *flvb* loci. *flva* LB/RB are amplified only in *flva* KO lines and *flvb* LB/RB only in *flvb* KO lines, while no PCR product was detected in WT, as expected. Amplification of *Actin* gene is also shown as a PCR positive control.

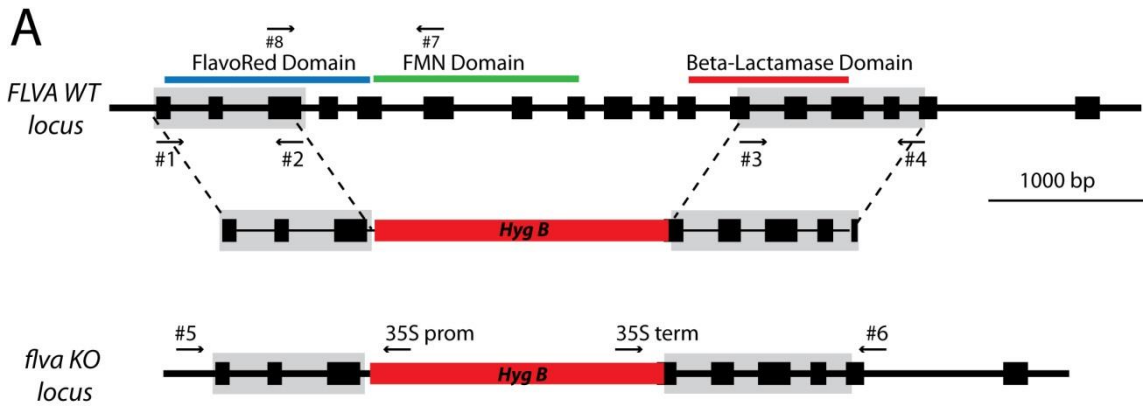

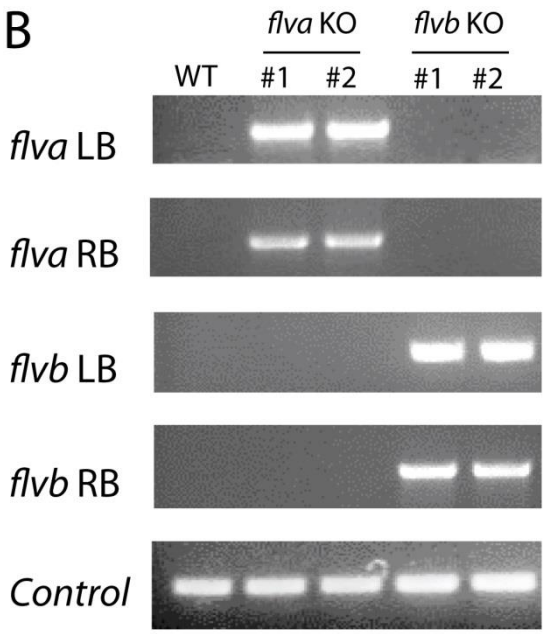

Figure S3. *P. patens flva* KO generation and screening.
The example of five independent *flva* KO lines is showed, but similar results were obtained also in the case of *flvb* KO plants. **A)** All the selected lines present the disruption of *FLVA* gene, verified with the PCR amplification of both left (LB) and right borders (RB) of the targeting construct. WT is also included as a negative control. **B)** In the same lines the loss of *FLVA* gene expression was verified by RT-PCR, with WT and a *flvb* KO mutant also included as controls. In A and B white lines indicate other lanes were present in the same gel. **C)** All the selected lines showed a slower Chl fluorescence quenching compared to control plants when actinic light is switched on (see also Fig. 3A). Chl fluorescence analyses were performed with a closed fluorescence imaging device (FluorCam, Photon System Instruments).

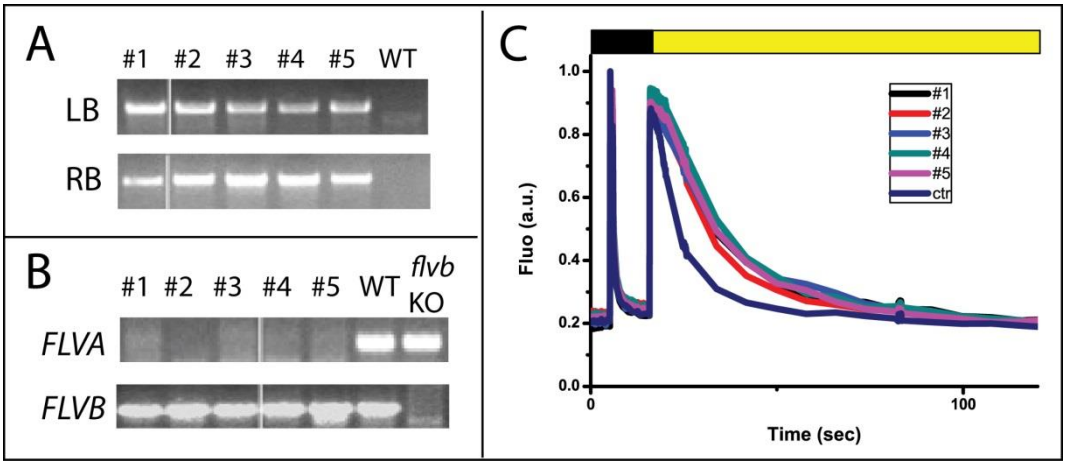

Figure S4. Electrochromic Shift (ECS) kinetics, estimation of functional PSI and PSII complexes and calculation of photosynthetic electron transport rate (ETR).

A) Representative kinetics of the ECS signal measured in intact tissues of *P. patens* upon excitation with a saturating xenon pulse. PS content was evaluated from single turnover flashes using a xenon lamp, which was applied at time t= 0 ms. Because of the flash length, double PSI turnovers take place, leading to over-estimation of PSI content by ≈ 40% (24). This effect, however, lowers the absolute values of ETR and PSI/PSII ratio but was verified to not alter the kinetics nor the differences between WT and mutants.

Measurements reported are from plants grown under fluctuating light for 7 days. Left panel WT; central panel *flva* KO; right panel *flvb* KO. Black dots represent control samples infiltrated only with buffer (HEPES 20mM pH 7.5, KCl 10mM), whereas white dots are from plants treated with 3-(3,4-dichlorophenyl)-1,1-dimethylurea (DCMU, 20μM) and hydroxylamine (HA, 4mM) to inhibit PSII charge separation. Each trace is the average of 15 scans given at 0.2 Hz. The blue lines indicate the level of PSII + PSI charge separation in samples infiltrated with buffer only and the red lines indicate the level PSI charge separation in DCMU/HA treated samples. The values presented here are normalized to PSII + PSI charge separation only for graphical purposes. The signal absolute values were used to calculate the stoichiometry of functional PSI and PSII reaction centres, which, considering the over-estimation of PSI for the xenon lamp, is therefore similarly under-estimated by ≈ 40% (Fig. 7A, Table S1).

B) Membrane potential changes induced by actinic light illumination and C) representative traces of changes in ECS signal to evaluate ETR. The analysis of changes in ECS during light-to-dark transition has been used to measure photosynthetic electron transport rate in a large variety of photosynthetic organisms at different developmental stages (22-26). ECS signal in fact depends on trans-thylakoid membrane potential that under light treatment is positively sustained by the activity of PSII, cytb_6f and PSI and negatively counteracted by ATPase proton pumping. Conversely, when light is switched off, PSII and PSI are inactivated and therefore the direct comparison between the ECS signals in the light and in the dark provide information on the electron transport rates of PSII and PSI. **B)** Example of ECS kinetic employed for calculation of total electron transport in *P. patens* (a representative kinetic from WT sample grown in control condition is shown, normalized per PSI turnovers). ECS signal induced by a continuous illumination was measured as the difference between ECS values at 520nm and 546nm, allowing to eliminate minor spectral and light scattering changes due to continuous illumination (25).Vertical dotted black bars indicate the different time points where actinic light was switched off for 30 ms to allow the calculation of the slope in the light (S_L) and the one in the dark (S_D). **C)** Detail of S_L and S_D calculation. The slope in the light (S_L, red) was calculated from the absolute signal amplitude in the last 20 ms in the light, while the slope in the dark (S_D, blue) was calculated in the time range 1.5-5.5 ms in the dark to avoid PSI charge recombination contribution immediately after light switch off (26). ETR was calculated as S_L-S_D and then normalized to the PSI turnovers (determined as in **A**). Considering the PSI over-estimation due to the use of xenon flash, the normalized ETR values are therefore under-estimated to the same extent of ≈ 40%, but this affects only the absolute e-/sec value, not the ETR time-dependent kinetics nor the differences between WT and *flv* KOs.

The analyses were repeated also in DCMU treated samples, where PSII is inactivated and therefore the difference in ECS signal in the light/dark periods is exclusively PSI-dependent and reflects the cyclic electron transport rates.

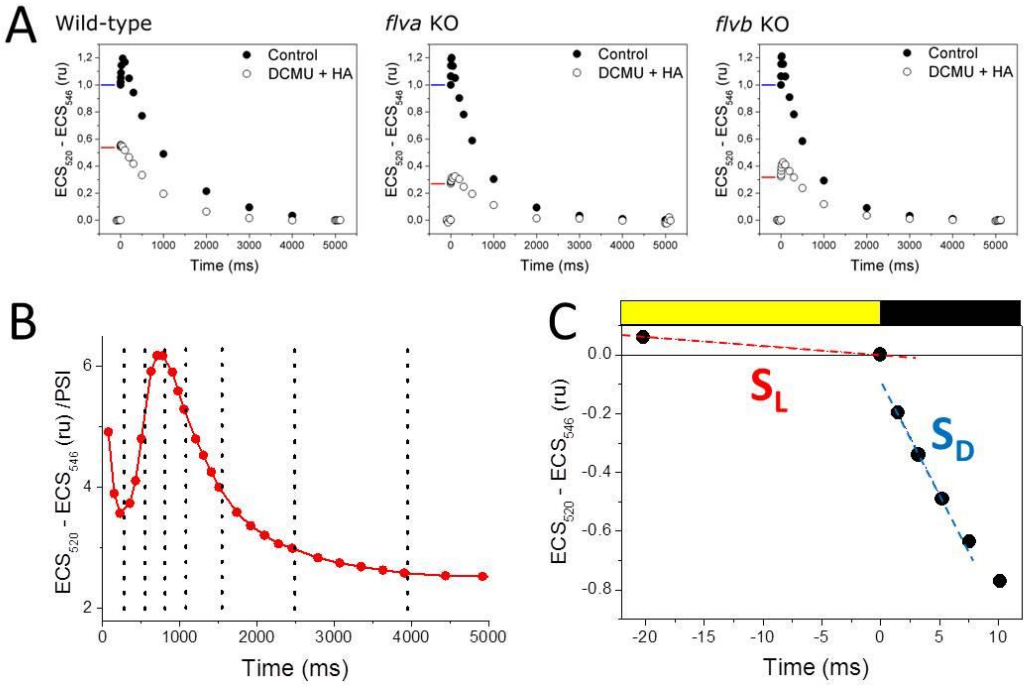
A
Wild-type
flva KO
flvb KO
Control
DCMU + HA
ECS520 - ECS546 (ru)
Time (ms)
B
ECS520 - ECS546 (ru) /PSI
Time (ms)
C
SL
SD
ECS520 - ECS546 (ru)
Time (ms)

Figure S5. Electron transport rate upon illumination with different actinic light intensities in control light grown plants.

Total electron transport rate (ETR) was evaluated in dark acclimated tissues *in vivo* using different actinic light intensities. **A)** Dependence of total photosynthetic electron transport rate on the actinic light employed in WT plants. Three different actinic light intensities were tested: 45 μmol photons m^{-2} s^{-1} (cyan squares), 150 μmol photons m^{-2} s^{-1} (orange triangles) and 940 μmol photons m^{-2} s^{-1} (black circles). The latter is also reported in Fig. 2A. **B)** ETR measured in WT (black), *flva* KO (red) and *flvb* KO (blue) plants illuminated with dim light (45 μmol photons m^{-2} s^{-1} actinic light).

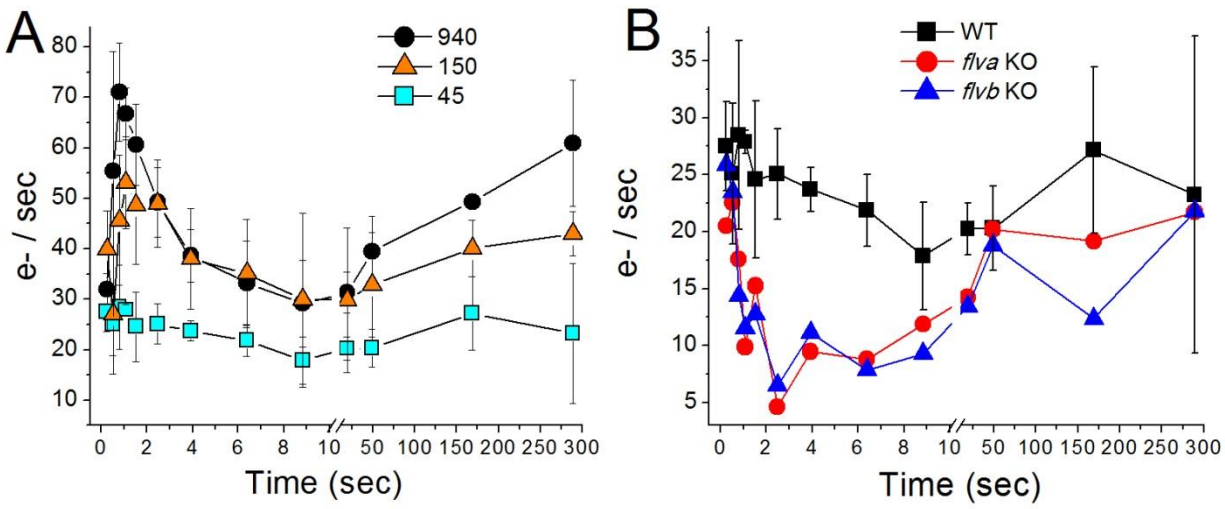

Figure S6. Quantitative estimation of the contribution of the different pathways on the total ETR in wild-type plants. Here the relative contributions of FLV dependent, linear and cyclic electron transport are estimated in WT and *flv* KO lines after 0.8 sec of illumination (peak of ETR in WT plants). Values are calculated from data presented in Fig. 2. The difference in ETR values between untreated samples of WT and *flv* KO mutants (black histograms, blue dashed line) shows a FLV-dependent transport. The comparison between untreated (black) vs. DCMU-treated (grey) samples instead gives an estimation of the contribution of cyclic electron flow on the total electron transport within each genotype (see red dashed line for WT), highlighting an increased contribution in *flv* KO.
Consequently, in WT the largest fraction of ETR is due to FLV with a contribution of cyclic electron transport. A residual contribution of linear ETR in WT can be either due to FLV or to linear transport to NADPH. In *flv* KOs, conversely, at this time point electron transport was only due to cyclic electron transport, as shown by the very similar values recorded in untreated (black) and DCMU treated (grey) samples.

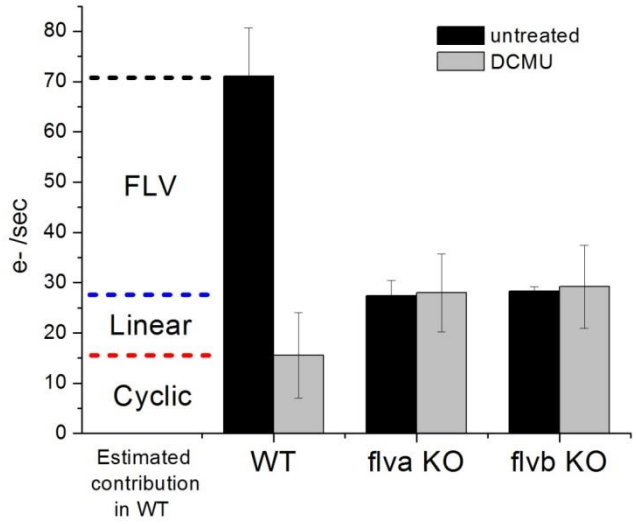

Figure S7. Additional data on Chl fluorescence Saturation pulse analyses.
Chl fluorescence quenching kinetics were obtained using the Dual-channel (Chl fluo and $P700^{+}$ absorption) slow kinetic analyses with Dual-PAM-100 (Walz) in control light grown tissues. After 40 min of dark acclimation, tissues were trasferred from plates to Glass fiber filters (Millipore) for the analyses. Here the complete light induction/dark recovery kinetic of the PSII quantum yield (Y(II)) **(A)**, Q_A relative reduction **(B)**, and non-photochemical energy dissipation as heat (NPQ) **(C)** are reported. In all panels, WT is shown in black, *flva* KO line in red and *flvb* KO line in blue. Values are reported as averages ± SD (n=4). Upper yellow bar indicates the phase where actinic light is on (175 µmol photons m^{-2} s^{-1}), black bar the dark phase. Selected part (0-150; 420-480 sec) of B and C panels are shown also in Fig. 3B-C.

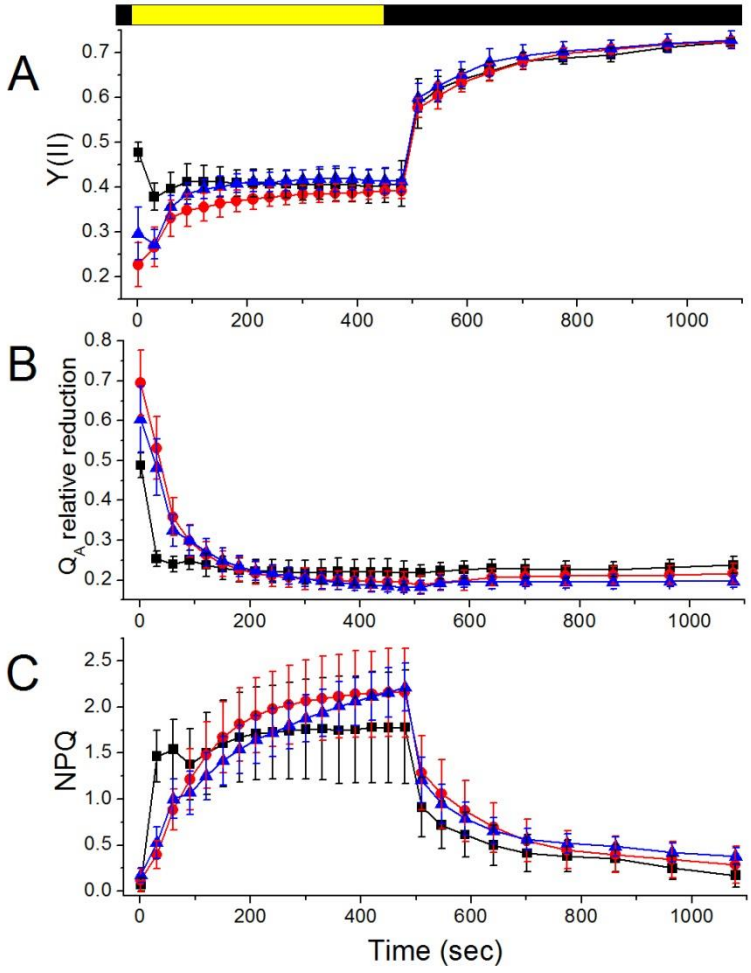

Figure S8. Verification of dependence of *flv* KO phenotype on the light intensity applied.
Analyses of PSII and PSI efficiencies on dark-acclimated moss tissues grown in control light (Chl fluorescence and $P700^+$ absorption signal analyses, respectively) were repeated using different actinic light intensities (50, 175 or 540 μmol photons m^{-2} s^{-1}). Detail of the first 2 minutes of illumination for PSII parameters Y(II) (PSII quantum yield), NPQ (non-photochemical quenching energy dissipation), relative Q_A reduction and PSI-related ones Y(I) (PSI quantum yield) and Y(NA) (PSI acceptor-side limitation) are reported. In all panels, WT is shown in black, *flva* KO line in red and *flvb* KO line in blue. Values are expressed as average ± SD of 3 (50 μmol photons m^{-2} s^{-1}) or 4 (175 and 540 μmol photons m^{-2} s^{-1}) independent replicates.

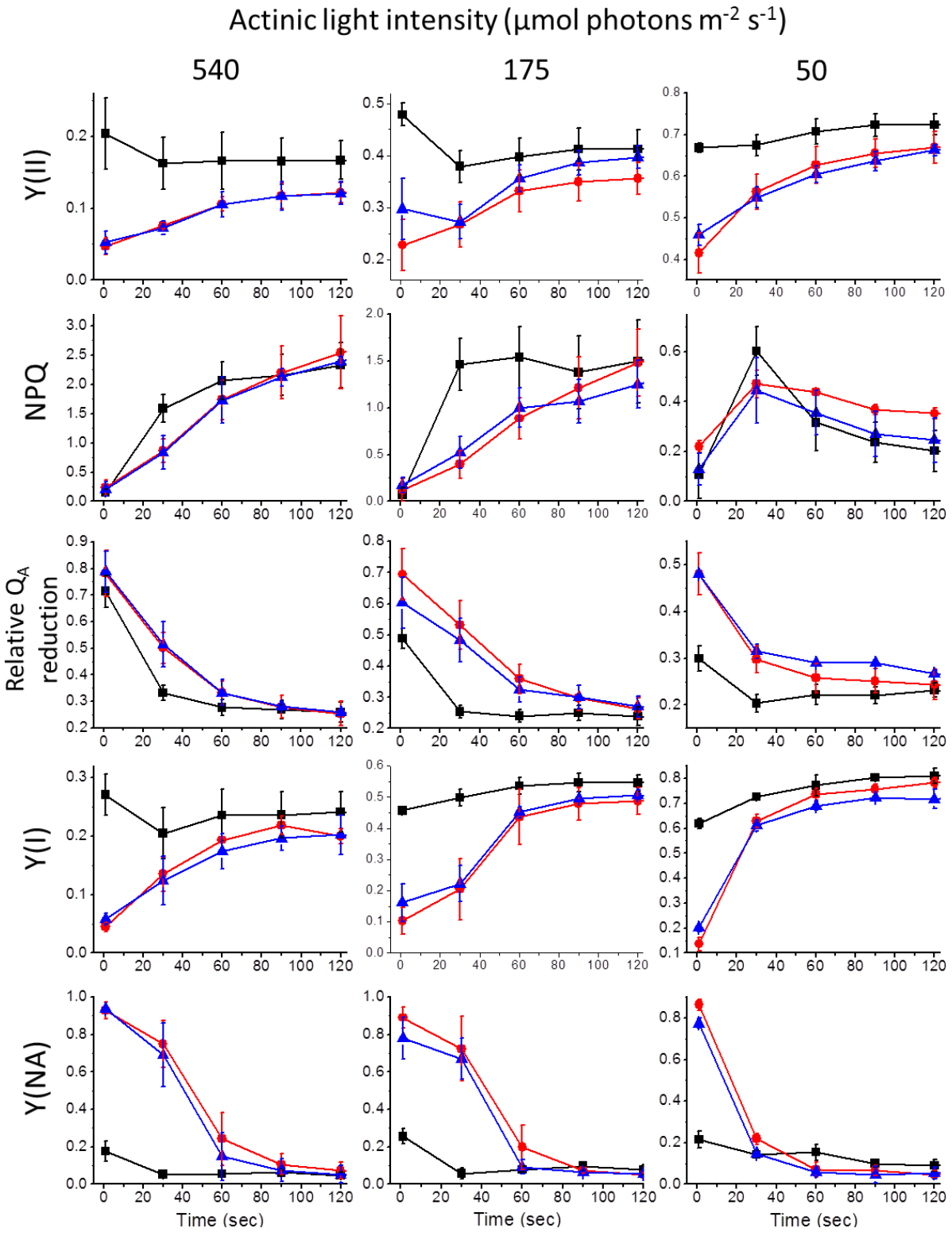

Figure S9. Complete light induction /dark recovery PSI kinetics.

P700^{+} absorption signal was monitored *in vivo* using the Dual-channel of Dual-PAM-100 (Walz) on mosses grown in control conditions and trasferred from plates to Glass fiber filters (Millipore). In the case of *flv* KO lines, the detection of maximum P700^{+} signal (Pm value) after 40 min of dark-acclimation required a 5 min treatment with mild light (50 µmol of photons m^{-2} s^{-1}), followed by a 5 min dark and then Pm was determined. Noteworthy, in the case of WT this light pre-treatment did not affect Pm value compared to the one detected after the first 40-min dark-acclimation. Here the complete light induction/dark recovery kinetic of the PSI parameters Y(I) **(A)**, Y(NA) **(B)** and Y(ND) **(C)** are reported. In all panels, WT is shown in black, *flva* KO line in red and *flvb* KO line in blue. Upper yellow bar indicate the phase where actinic light is on (540 µmol photons m^{-2} s^{-1}), black bar the dark phase. Selected part (0-150; 420-480 sec) of these kinetics are shown also in Fig. 4.

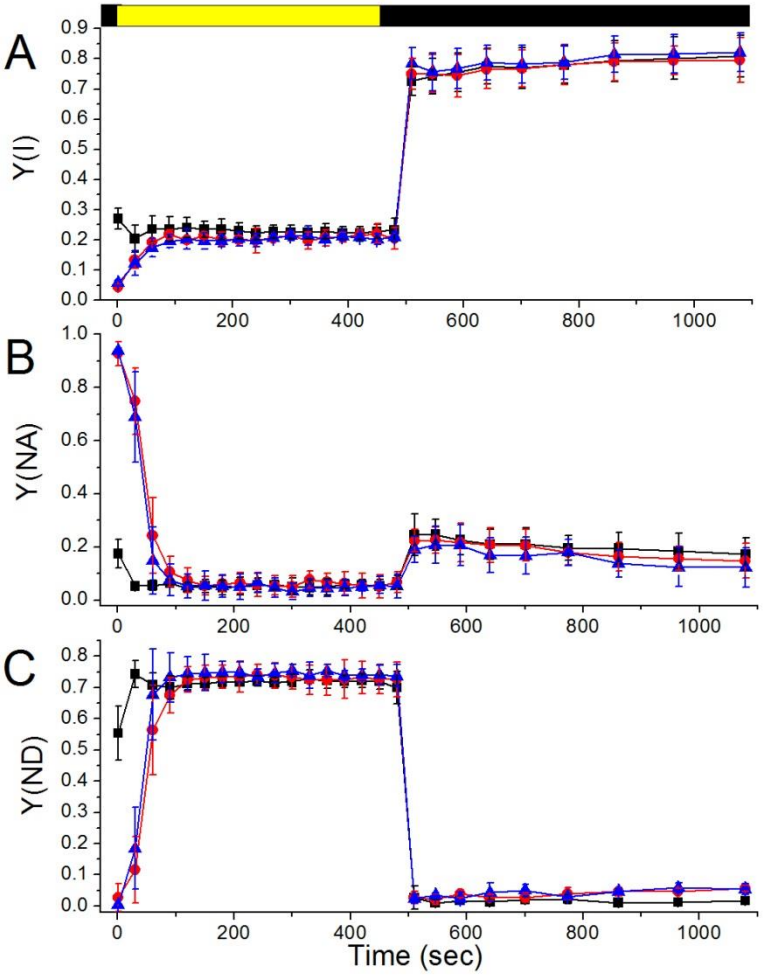

Figure S10. Effects of methylviologen on $P700^+$ and Chl fluorescence signals in WT and *flv* KO lines.
Tissues from WT and *flv* KO plants grown for 10 days under control light conditions were treated with 0.1mM methylviologen (MV) for 10 min in darkness before the measurements.
A-F) Effect of MV on WT and mutant lines. In each panel MV-treated samples are shown in black while control samples, incubated with HEPES/sorbitol buffer only, are shown in red. $P700^+$ absorption signals (A, C, E) were normalized to the steady state signal, while Chl fluorescence (B, D, F) to the maximum dark-acclimated fluorescence (Fm). Analyses were performed in the same experimental conditions as described in Figure 4 (actinic light 540 µmol photons m^{-2} s^{-1}).
G-H) Restoration of *flv* KO phenotype by MV. WT signals (black) together with signals from MV treated *flv* KO plants (*flva* KO in blue and *flvb* KO in green). The MV treatment almost completely rescued mutant phenotype to the wild-type levels. $P700^+$ signal of *flv* KO mutants raised rapidly upon illumination as in WT after the addition of MV, and also Chl fluorescence quenching was stronger and faster in *flv* KO lines when an alternative electron acceptor was given to the plants.

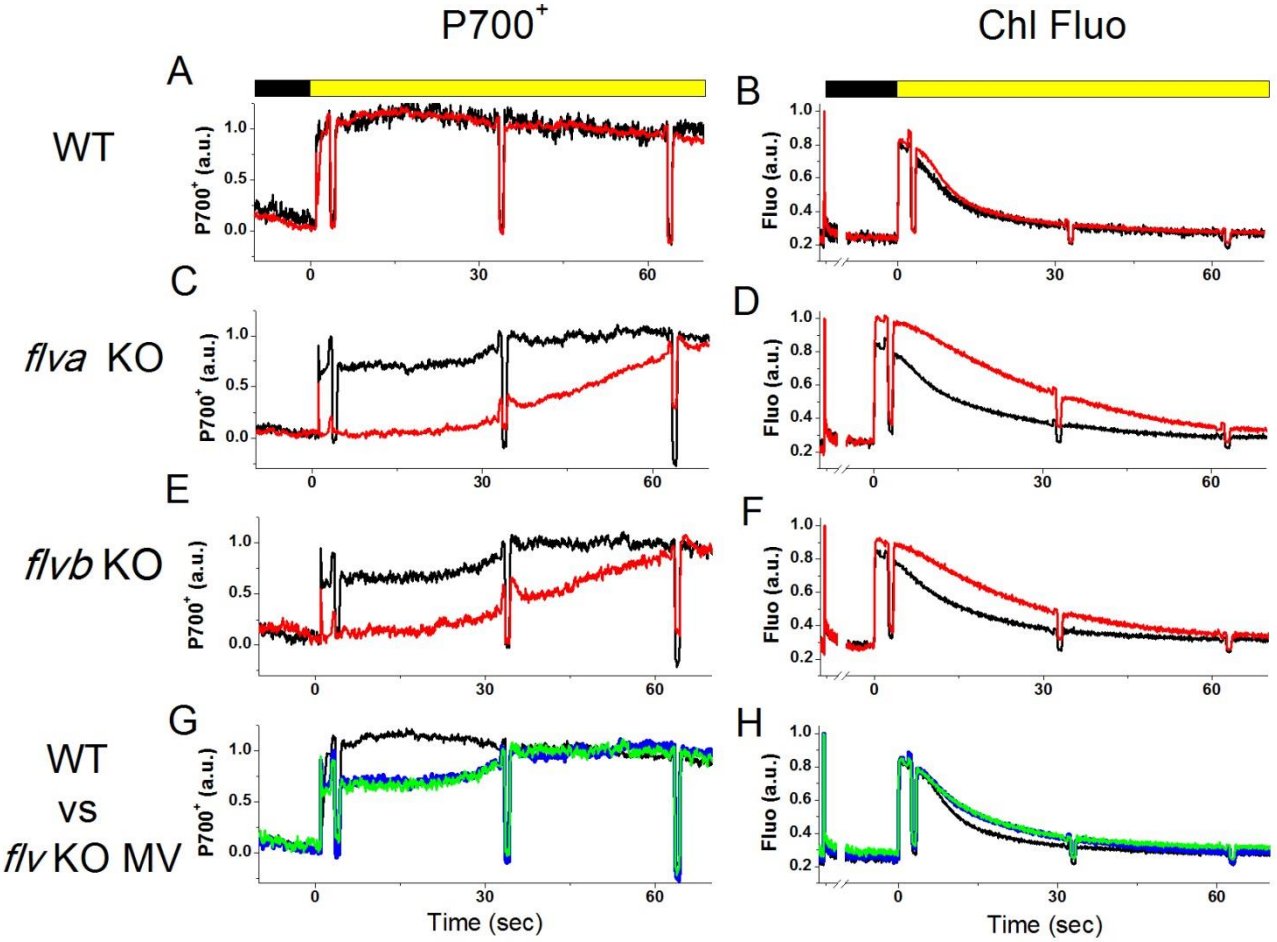

Figure S11. PSI and PSII quantum yields and heat dissipation in mosses treated with fluctuating light.
Chl fluorescence quenching and $P700^{+}$ absorption signal were monitored simultaneously in response to variable illumination in WT and *flv* KO mutants lines. In addition to the parameters shown in Fig. 5, here PSII quantum yield (Y(II)), energy dissipation as heat (NPQ) and PSI quantum yield (Y(I)) are reported in **A, B** and **C**, respectively. In all panels, WT is shown in black, *flva* KO in red and *flvb* KO in blue. Orange upper bars indicate the illumination with dim actinic light, yellow bars and shading the phases where saturating actinic light was employed.

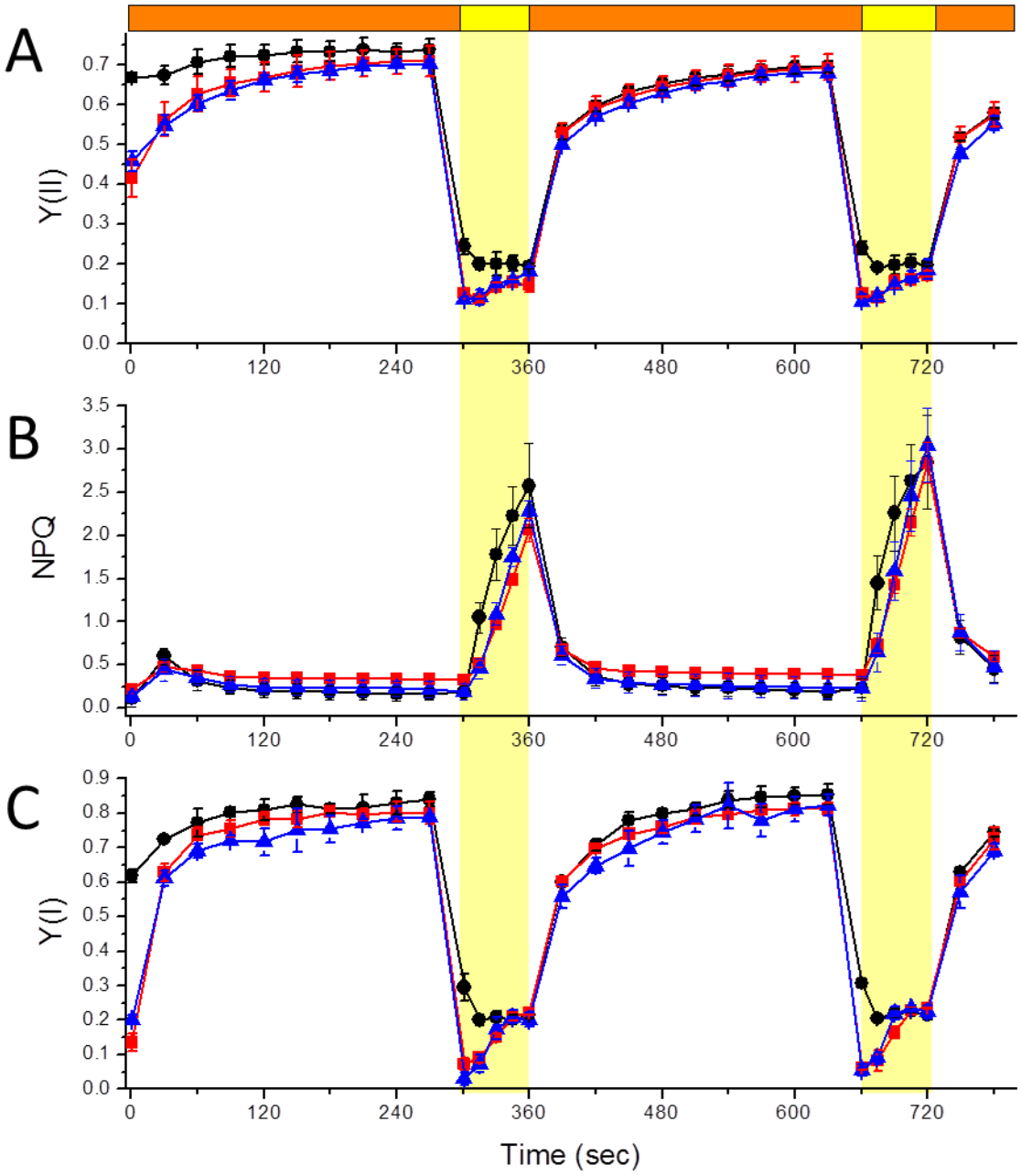

Figure S12. PsaD and D2 accumulation during 2 weeks of FL treatment.
Western blotting analysis on 2 weeks-treated FL plants (FL) and control plants from the continuous light (CL). The immunodetection of the PSI subunit PsaD and PSII subunit D2 shows the same trend observed after 1-week FL treatment (Figure 7B). 1 Chl μg of thylakoid extracts was loaded in each lane.

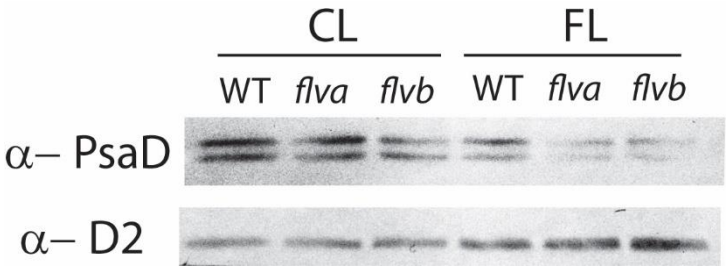

Figure S13. ECS change kinetics in *Physcomitrella patens* plants. A) Membrane potential was measured on dark-acclimated moss tissues grown in control light and treated with saturating light (940 μmol photons m^{-2} s^{-1}). WT plants (black) are characterised by a fast increase of the membrane potential that peaked in the first second after switching the light on. Conversely, in the case of *flva* KO (red) and *flvb* KO (blue) mutants, after the initial decrease, the membrane potential stalled. Then, after 6 sec of light, values from the three genotypes were similar. Representative kinetics for each genotype are shown here, but they are confirmed by at least other 3 independent replicates. B) The two components of the proton motif force (ΔΨ and ΔpH, red arrows on the right side) were measured by treating the plants for 1 second with actinic light. After switching the light off, a fast decay (i.e. the total proton motif force) followed by a slower rise phase (ΔpH) are seen in wild-type plants. The ΔpH component is not detectable in *flva* and *flvb* KO mutants. Black and yellow bars on top represent the dark and light phases. Traces are the average of three independent samples.

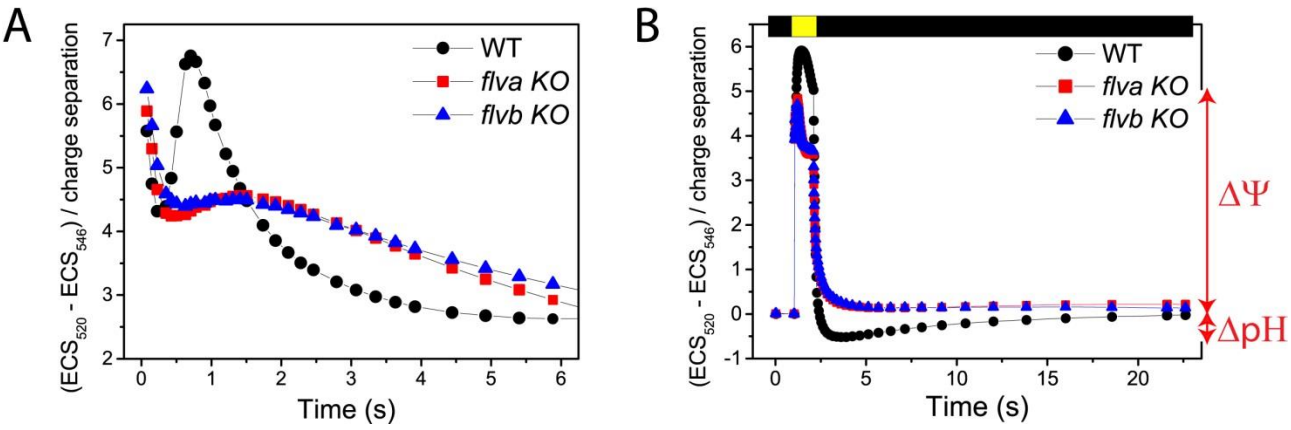

Table S1. PSI, PSII and pigment binding properties in WT and *flv* KO lines grown in control and fluctuating light conditions.

PSII quantum yield (Fv/Fm), PSI maximal signal (Pm, proportional to the amount of oxidizable P700 in the sample) and PSI/PSII ratio were evaluated *in vivo* in WT, *flva* KO and *flvb* KO lines grown in control (CL) or fluctuating light conditions (FL). For Pm determination, tissues containing 13 ± 2 µg Chl were analysed. In the same samples also pigment content (Chl a/b and Chl/Car ratios) was evaluated.

All values are expressed as average ± SD of 3 independent replicates. Asterisks indicate values significantly different from WT (t test, p=0.01).

	Fv/Fm	Pm	PSI/PSII	Chla/b	Chl/Car
WT CL	0.79 ± 0.02	0.22± 0.04	1.29 ± 0.19	2.58 ±0.14	3.68 ± 0.19
***flva* KO CL**	0.78 ±0.02	0.23 ± 0.06	1.26± 0.19	2.65 ±0.03	3.48 ±0.16
***flvb* KO CL**	0.78 ±0.01	0.25 ± 0.02	1.31 ± 0.16	2.71 ±0.05	3.53 ±0.06
WT FL	0.78 ±0.02	0.29 ± 0.04	1.09 ± 0.27	2.60 ±0.08	3.36 ±0.32
***flva* KO FL**	0.68 ±0.04 **	0.05 ± 0.01 **	0.40 ± 0.02 **	2.51 ±0.08	3.11 ±0.18
***flvb* KO FL**	0.70 ±0.04 **	0.07 ± 0.02 **	0.48 ± 0.02 **	2.69±0.08	3.05±0.31

Table S2. Primers employed for *flva* KO and *flvb* KO generation and screening.

The table reports all the primers used to generate and characterize *flva* KO and *flvb* KO *P. patens* lines. Sequences homologous to *P. patens* genome are reported in capital letters, restriction enzymes sequences as underlined. For both *FLVA* (XP_001759251.1) and *FLVB* (XP_001756079.1) loci, the primers were designed to disrupt the coding sequence with the insertion of the resistance cassette. Genomic DNA from WT strain (obtained with EuroGOLD Plant DNA mini kit, EuroClone) was used as a template to amplify selected homologous regions. All the PCR products were first cloned into pGEM T-easy vector (Promega), to be then digested and cloned into the final vector for moss transformation.

Primers flva#1 and 2 were used to amplify *FLVA* homologous region which was cloned, after digestion with HindIII-BsiWI endonucleases, upstream the Hygromicin B (HygB) resistance cassette into BHRf plasmid. Primers flva#3 and 4 instead amplified the downstream homologous region, cloned into the same vector after digestion with NotI/SalI restriction enzymes (*flva* KO vector). Moss protoplasts were transformed with *flva* KO construct linearized with AvrII/SpeI. After transformation and two round of selection, homologous recombination in HygB resistant lines was evaluated. Primers flva#5 (forward)/ 35S promoter (reverse) and 35S terminator (for)/ flva#6 (rev) allowed to amplify Left (LB) and Right Border (RB), respectively, of the integrated cassette in *flva* KO lines (see Fig. S2B and S3A). Primers #5 and #6 are designed to anneal in the genomic region external to the target recombination regions, while primers 35S promoter/terminator anneal in the integrated resistance cassette. Therefore, only lines harbouring the homologous recombination in *FLVA* locus produce amplicons. Finally, primers flva#7and 8 allowed to check *FLVA* expression on cDNA by RT-PCR.

A very similar approach was used for *flvb* KO generation. Primers flvB#1 and 2 allowed to amplify *FLVB* gene region cloned upstream of G418 resistance cassette in BNRf plasmid after digestion with SalI/BsiWI; primers flvb#3 and 4 and then digestion with SacII/SpeI allowed to clone downstream FLVB region generating *flvb* KO construct in BNRf vector. Protoplasts were transformed with *flvb* KO cassette digested with SalI/SpeI. After transformation and selection, primers flvb#5 / HNZupRev allowed to amplify LB, and 35S terminator/flvb#6 the RB of the resistant lines. Primers flvb#7 and 8 were used to check *FLVB* expression on cDNA.

Actin FOR and REV were used as PCR controls both for genomic DNA and cDNA templates.

Gene	Primer Name	Sequence	Use
PpFlva	FlvA_1 (HindIII)	tatccctaggcggaccgAAGCTTTACAGGGCCATTACAGG	KO generation
	FlvA_2 (BsiWI)	gttatctcgagtcgcgacgtaCGGCAGTTCACTGAAGAAATAAG	KO generation
	FlvA_3 (NotI)	taccgagctcgaattcgcggccGCAGGATCATAAACACACAAGC	KO generation
	FlvA_4(SpeI)	atatcacgcgtggcgccactaGTGCGTGTTAACTTAGAGAGG	KO generation
	FlvA_5	CACACTCTACATCGAAGCCTCA	KO screening
	FlvA_6	GCTAAGCGCAGCAACACTTT	KO screening
	FlvA_7	TTTGGCTCTTTCGGGTGGAG	RT-PCR
	FlvA_8	GACGGTTTTCGCCAGGTTTG	RT-PCR
PpFlvB	FlvB_1 (SalI)	agcttgcatgcctgcaggtcgACATCCTATTTACAAACTCTTAT	KO generation
	FlvB_2 (BsiWI)	gttatctcgagtcgcgacgtacgTAACCGGAACAAAACAATG	KO generation
	FlvB_3 (SacII)	gctcgaattcgcggccgcGGGTGAAAGTTCTCAAACCAAG	KO generation
	FlvB_4 (SpeI)	atatcacgcgtggcgccACTAGTGGGCCTCGTGAATTC	KO generation
	FlvB_5	TTCCTTGTGCAGATTTAAAGGCA	KO screening
	FlvB_6	AGGTTCCACCCACCGAGATA	KO screening
	FlvB_7	CTGTCAAAGCCAAGCAACCC	RT-PCR
	FlvB_8	AGGACTTCCATTTGCCCCAG	RT-PCR
35S	35S promoter	GTGTCGTGCTCCACCATGT	Flva KO screening
	NHZupRev	CCAGTCTTTACGGCGAGTTC	Flvb KO screening
	35S terminator	CGCTGAAATCACCAGTCTCTCT	KO screening
Actin	ACTIN2F	GCGAAGAGCGAGTATGACGAG	RT-PCR
	ACTIN2R	AGCCACGAATCTAACTTGTGATG	RT-PCR